nature genetics

Fras1 deficiency results in cryptophthalmos, renal agenesis and blebbed phenotype in mice

Sophia Vrontou[1,2], Petros Petrou[1], Barbara I Meyer[3], Vassilis K Galanopoulos[2], Kenji Imai[4], Masayuki Yanagi[4], Kamal Chowdhury[3], Peter J Scambler[5] & Georges Chalepakis[1,2]

Loss of tight association between epidermis and dermis underlies several blistering disorders and is frequently caused by impaired function of extracellular matrix (ECM) proteins[1,2]. Here we describe a new protein in mouse, Fras1, that is specifically detected in a linear fashion underlying the epidermis and the basal surface of other epithelia in embryos. Loss of Fras1 function results in the formation of subepidermal hemorrhagic blisters as well as unilateral or bilateral renal agenesis during mouse embryogenesis. Postnatally, homozygous *Fras1* mutants have fusion of the eyelids and digits and unilateral renal agenesis or dysplasia. The defects observed in *Fras1*$^{-/-}$ mice phenocopy those of the existing *bl* (blebbed) mouse mutants[3,4], which have been considered a model for the human genetic disorder Fraser syndrome[5,6]. We show that *bl*/*bl* homozygous embryos are devoid of Fras1 protein, consistent with the finding that *Fras1* is mutated in these mice[6]. In sum, our data suggest that perturbations in the composition of the extracellular space underlying epithelia could account for the onset of the blebbed phenotype in mouse and Fraser syndrome manifestation in human.

The isolated *Fras1* cDNA encompasses 15,865 bp, and the longest open reading frame encodes a protein of 4,010 amino acids that contains a signal peptide and a predicted transmembrane domain at the C terminus. The protein can be subdivided into several distinct domains found in different proteins, such as the C-domain of von Willebrand factor (VWC; ref. 7), the cysteine-rich motifs of furin proteases[8], the chondroitin sulfate proteoglycan core protein NG2 (ref. 9) and the calcium-binding loop of Na^+-Ca^{2+} exchange proteins[10] (**Fig. 1a**). Fras1 has the highest sequence identity (32%) with the ECM3 protein from sea urchin[11] that lacks the cysteine-rich domains. Northern-blot analysis identified one transcript corresponding to almost the complete cDNA sequence (15–16 kb) and a smaller transcript of 4.8 kb (**Fig. 1b**). We mapped *Fras1* to mouse chromosome 5 near *D5Mit20* and the human homolog *FRAS1* to a homologous region on human chromosome 4q13–q21 near the sequence-tagged sites SHGC-20205 and SHGC-1003.

We assessed *Fras1* expression by RNA *in situ* hybridization. *Fras1* transcripts were detected in the epidermal epithelium (**Fig. 1c**,**d**) but also in epithelia of several developing organs, such as gut and stomach (data not shown), and internal epithelia of the metanephros (**Fig. 1e**). Consistent with the epithelial origin of *Fras1* mRNA, Fras1 immunoreactivity produced a linear staining pattern at the basal surface of epithelia, as in the dermal-epidermal junction (DEJ; **Fig. 1f**), the gut (**Fig. 1g**) and the outgrowing ureteric bud (**Fig. 1h**).

To study the function of *Fras1*, we generated a mutated allele by homologous recombination in mouse embryonic stem cells (**Figs. 1a** and **2a**) and verified correct targeting at the 5′ end and the integrity of the locus at the 3′ end by Southern blotting (**Fig. 2b**,**c**). Interbreeding of heterozygous mice on the C57BL/10 background did not yield any living homozygous mutants; further analysis identified the onset of the abnormal phenotype of *Fras1*$^{-/-}$ embryos around embryonic day (E) 12.0. This phenotype occurs as subepidermal blisters predominantly formed in the head region around the eyes and at the distal part of the limbs (**Fig. 3**). As development proceeds, blisters that are initially transparent gradually become hemorrhagic, and homozygous embryos die between E14.5 and E16.5. Contrary to the known human skin blistering disorders and existing mouse models, in which blister formation is usually induced by mechanical trauma or friction in neonates or adults[1,12–14], the exceptionally large blisters in *Fras1*$^{-/-}$ embryos develop *in utero*. Formation of blisters in *Fras1*$^{-/-}$ embryos might result from a combination of epidermal fragility and mechanical friction of the head and distal limbs, which are in close contact with the uterine wall. Blisters over the eye probably exert a mechanical pressure leading to local deformations of the affected areas (**Fig. 3a**,**d**,**e**), although normal development of eye structures does not seem to be affected (**Fig. 3e**). *Fras1*$^{+/-}$ embryos appeared normal and were indistinguishable from their wild-type littermates.

Fras1$^{-/-}$ mutants on the NMRI background have an identical, though occasionally slightly milder, phenotype that allows some embryos (50%) to develop to term, half of which survive to adulthood and are fertile. Newborn homozygous mice usually bear preformed blisters at the distal limbs that gradually resolve. We have

[1]Institute of Molecular Biology and Biotechnology, FO.R.T.H., Heraklion 71110, Crete, Greece. [2]Department of Biology, University of Crete, Heraklion 71409, Crete, Greece. [3]Max-Planck-Institute of Biophysical Chemistry, Department of Molecular Cell Biology, Am Fassberg 11, D-37077 Goettingen, Germany. [4]GSF-National Research Center for Environment and Health, Institute of Developmental Genetics, Neuherberg, Germany. [5]Molecular Medicine, Unit, Institute of Child Health, London WC1N 1EH, UK. Correspondence should be addressed to G.C. (chalepak@imbb.forth.gr).

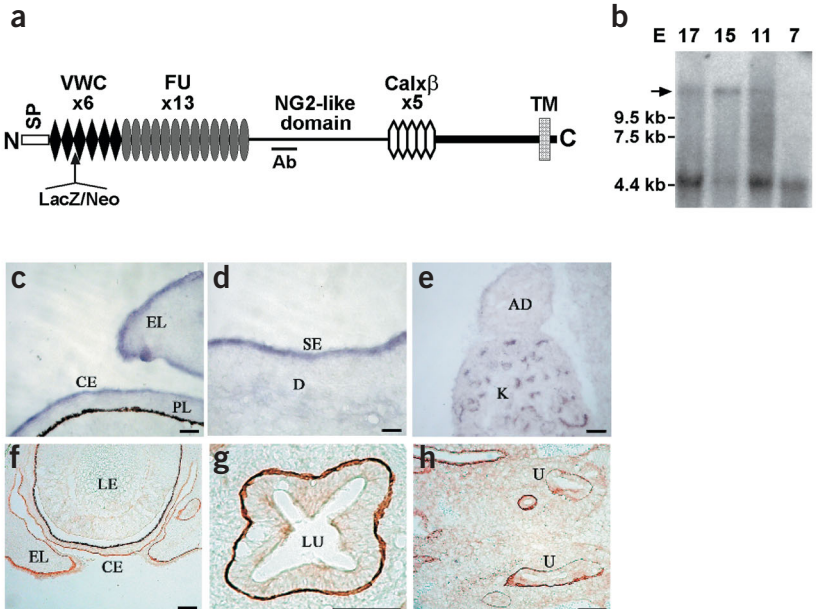

Figure 1 Schematic representation of Fras1 and detection of the mRNA and protein. (**a**) The different domains of Fras1 are predicted from deduced amino acid sequence. Beginning from the N-terminal end of the protein, a signal peptide (SP, amino acids 2–22) is encountered first, followed by six repeated cysteine-rich motifs similar to those of VWC (amino acids 27–417), 13 cysteine motifs found in furin proteases (FU, amino acids 418–1,095), a region homologous to NG2 chondroitin sulfate proteoglycan (amino acids 1,104–2,520), five tandem calcium binding motifs of Na^{+}-Ca^{+2} exchange proteins (Calxβ, amino acids 2,566–3,130) and a transmembrane domain (TM, amino acids 3,895–3,924) close to the C terminus. Arrow in front of the third VWC motif indicates the insertion site of the targeting vector used for the generation of the mutated allele. The protein domain used for immunization and polyclonal antibody production (Ab) is indicated by a bar. (**b**) Northern-blot analysis of *Fras1* mRNA. The blot contains poly(A)$^{+}$ RNA from four mouse embryonic developmental stages. Two transcripts of approximately 15–16 kb (arrow) and 4.8 kb are detected. The size of the larger transcript corresponds approximately to the sequenced cDNA (15,865 bp) deposited in the database. Numbers at the left side of the blot refer to RNA size markers. (**c**–**e**) Detection of *Fras1* RNA by *in situ* hybridization of transverse (**c**,**d**) and sagittal (**e**) cryosections of E14.5 wild-type embryos. Shown is the expression of *Fras1* in cornea (CE) and eyelid (EL) epithelium (**c**), in the skin epithelium (SE; **d**) and in the internal epithelia of the developing kidney (K; **e**). AD, adrenal gland; D, dermis; PL, pigment layer of the retina. (**f**) Immunoperoxidase staining with a specific antiserum detects Fras1 protein at the basal surface of cornea epithelium (CE) and eyelid epithelium (EL) on a sagittal section of E14.5 mouse embryo. LE, lens. (**g**) Transverse section of an E16.5 embryo showing Fras1 localization at the basal surface of enteric epithelium. LU, lumen of the gut. (**h**) Fras1-specific antibodies label the basal part of the epithelia sheets of ureter (U) on a transverse section of an E11.5 embryo. Scale bar in **c**,**d**, 40 μm; in **e**, 150 μm; and in **f**–**h**, 100 μm.

never observed large hemorrhagic blisters in the head region over the eyes in newborns, suggesting that these may lead to embryonic lethality. The external phenotypic features of the living homozygotes include the permanent fusion of one or both eyelids and of some or all digits (**Fig. 4a–f**). We found no significant changes in the number of apoptotic cells in the interdigital spaces of *Fras1*$^{-/-}$ limbs, indicating that defective apoptosis is not the primary cause of these fusions (data not shown). No indication for epidermal fragility, such as a new blister formation, has ever been observed postnatally, suggesting that these deformities are established during embryonic development and maintained through adulthood. This is supported by the fact that the function of Fras1 is restricted to embryonic development, as Fras1 is no longer detected in the epidermis of adult mice (data not shown).

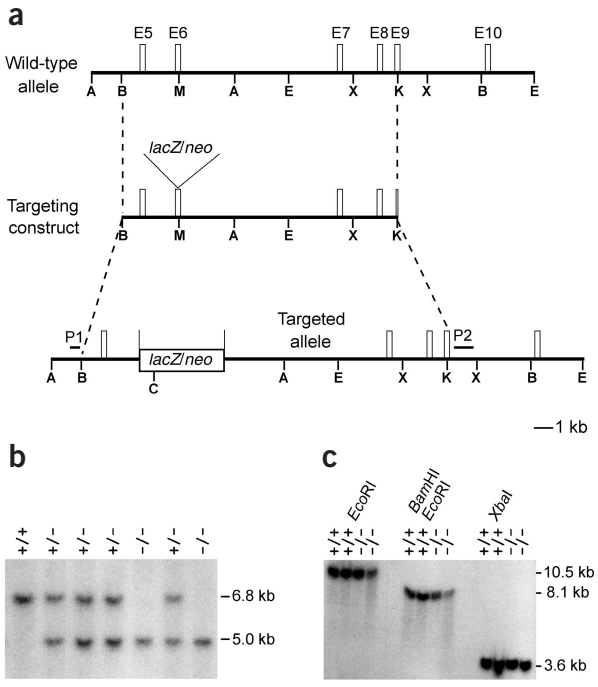

Figure 2 Targeted disruption of *Fras1*. (**a**) Schematic representation and partial restriction map of the mouse *Fras1* locus encompassing exons (E) 5–10. Open boxes represent exons numbered according to sequence comparison of the *Fras1* cDNA and the corresponding mouse genomic sequences in the Celera database. We inserted the *lacZ/neo* cassette into the *Msc*I restriction site of exon 6 in a sequence corresponding to amino acid 162. The *Fras1* genomic sequences that we used in the targeting construct are shown by dotted lines. A, *Apa*I; B, *Bam*HI; E, *Eco*RI; K, *Kpn*I; M, *Msc*I; X, *Xba*I. The positions of external probes that we used to monitor correct targeting event at the 5′ end (probe P1) and the integrity of the *Fras1* locus at the 3′ end (probe P2) are also shown. (**b**) Visualization of correct targeting by Southern-blot analysis. We hybridized genomic DNA digested with *Apa*I and *Cla*I from the offspring of *Fras1*$^{+/-}$ intercrosses with probe P1. A fragment of 5.0 kb instead of 6.8 kb is generated after proper integration of the targeting vector. The presence of both fragments identifies heterozygous offspring, whereas the detection of only the 5.0-kb or the 6.8-kb fragment indicates homozygous or wild-type offspring, respectively. (**c**) Southern-blot analysis of genomic DNA from wild-type and *Fras1*$^{-/-}$ offspring digested with *Eco*RI, *Bam*HI and *Eco*RI, or *Xba*I and probed with P2. We detected the same DNA fragments in each digestion regardless of the genotype, indicating that the integrity of the locus at the 3′ end is maintained after homologous recombination.

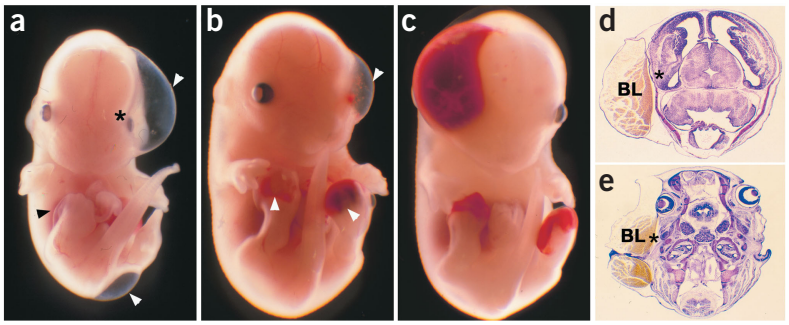

Figure 3 Onset and progression of blister formation in *Fras1*$^{-/-}$ embryos on the C57BL/10 background. (**a**) An E12.5 *Fras1*$^{-/-}$ embryo with three transparent blisters (arrowheads): at the right hindlimb, around the left eye and at the lower back. Asterisk indicates mechanical distortions caused by the blister. (**b**) At stage E13.5 hemorrhage in blisters becomes apparent. (**c**) Blood-filled blisters over the eye and the distal hindlimbs of an E14.5 embryo. (**d**,**e**) Cresyl violet staining of transverse sections from an E14.5 *Fras1*$^{-/-}$ embryo through the head. The formation of the blister (BL) at the right side of the head leads to mechanical distortions of the juxtaposed structures (asterisk). Development of eye structures, covered by the blister, does not seem to be affected (**e**).

Fras1$^{-/-}$ mutants in both backgrounds are further characterized by unilateral or bilateral renal agenesis or dysgenesis and hypoplasia (**Fig. 4g–j**). Metanephric kidney development is dependent on inductive interactions between the epithelium of the ureteric bud and the adjacent mesenchyme, in which several growth factors and ECM proteins have been implicated[15–17]. Notably, Fras1 was detected in the ECM underlying the basal surface of the outgrowing ureter (**Fig. 1h**) and a blind-ended ureter is present in newborn homozygotes with unilateral renal agenesis (**Fig. 4i**). This suggests that metanephric development in homozygous mutants is not disturbed at the stage of ureteric bud outgrowth but probably at the subsequent epithelial-mesenchymal interactions.

Given the specific localization of Fras1 at the DEJ and the blister formation in *Fras1*$^{-/-}$ embryos, we compared the composition and distribution of ECM proteins at the DEJ of wild-type and mutant embryos. Fras1-specific antibodies detected the protein underlying the epidermis in wild-type embryos and verified its absence in homozygous mutants (**Fig. 5a**,**b**). Staining for basement membrane zone (BMZ) markers such as laminin α5 and collagen VII indicated no significant alterations in the fluorescence pattern in *Fras1*$^{-/-}$ embryos in nonlesional epidermal regions as compared with wild-type controls (**Fig. 5c–f**). This suggests that there were no severe ruptures of the BMZ in *Fras1*$^{-/-}$ mutants. Staining for collagen VI, however, which is normally localized at the dermal side of the skin BMZ and in the connective tissue, did not indicate any visible deposition of this protein in the BMZ of *Fras1*$^{-/-}$ mutants (**Fig. 5g**,**h**). The loss of collagen VI deposition at the dermal side of the skin BMZ could be explained by a potential direct interaction between collagen VI and Fras1 that is abolished in *Fras1*$^{-/-}$ mutants. Notably, the central domain of Fras1 is related to chondroitin sulfate proteoglycan core protein NG2, which has been shown to interact *in vitro* with collagen types V and VI[18].

We then used BMZ markers to determine the plane in which tissue separation occurs on blister formation (**Fig. 6**). Histological staining showed that the blister cavity was enclosed only by epithelial cells at the tip of the blister roof (**Fig. 6b**). BMZ markers

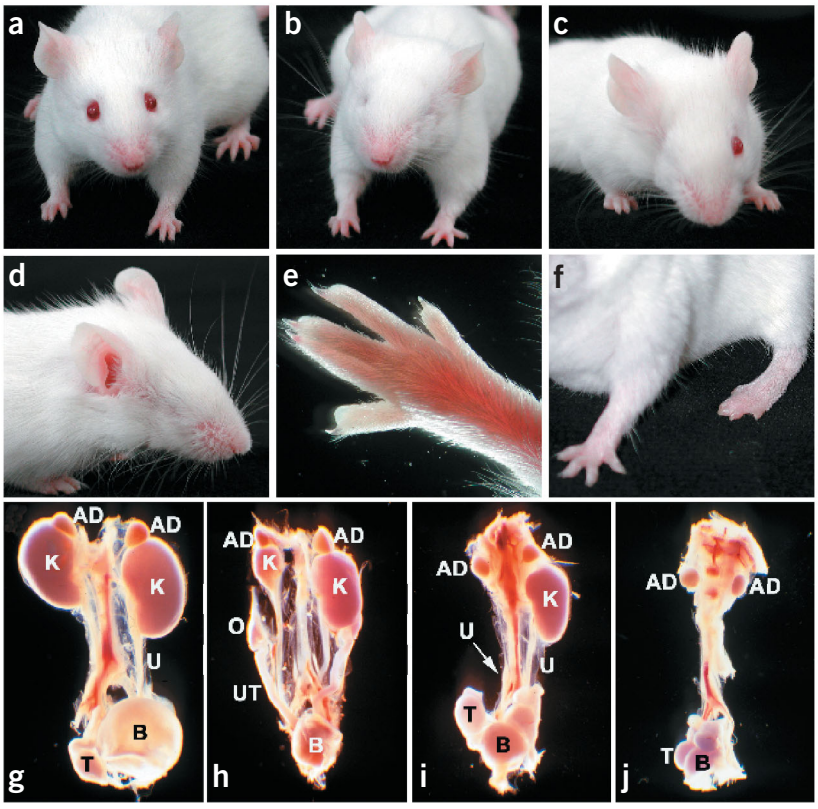

Figure 4 *Fras1*$^{-/-}$ mice on the NMRI background have fusions of eyelids and digits as well as renal agenesis or dysgenesis. (**a**) Frontal view of a wild-type mouse. (**b**) Approximately 20% of *Fras1*$^{-/-}$ mice have bilaterally closed eyelids. (**c**) About 75% of the mice have only one eyelid closed. The remaining 5% have a smaller eyelid opening. (**d**) Right lateral head view of the mouse shown in **c**. (**e**) A rare type of syndactyly observed in only 2% of the homozygous mutants. (**f**) A *Fras1*$^{-/-}$ mouse with complete fusion of the digits of the left hindlimb but phenotypically normal digits in the left forelimb. Homozygous mutant mice with no obvious abnormalities at the limb extremities accounted for approximately 10% of the cases (percentages are derived from the analyses of approximately 160 living mutants). (**g**) The urogenital system of a newborn wild-type male. Dissection of the urogenital system of *Fras1*$^{-/-}$ mice showed either unilateral kidney hypoplasia (**h**) or agenesis (**i**). In the latter case, a blind-ending ureter was evident at the side of renal agenesis (arrow in **i**). (**j**) Bilateral renal agenesis with no evidence of ureter formation in a *Fras1*$^{-/-}$ newborn male. In all cases, adrenal glands and gonads had normal macroscopical appearance. In general, *Fras1*$^{-/-}$ mice have different combinations of renal agenesis or dysgenesis. Histological analysis of E15.5 homozygous embryos showed either bilateral or unilateral lack of kidneys in approximately 50% of cases (17 of 35). AD, adrenal gland; B, bladder; K, kidney; O, ovary; T, testis; U, ureter; UT, uterus.

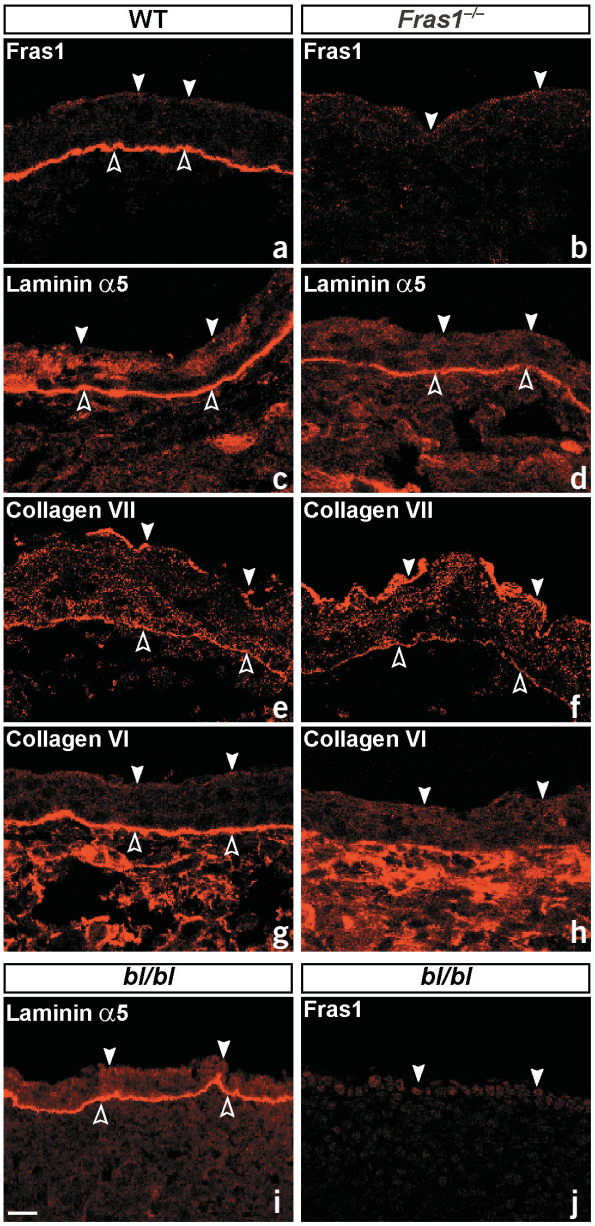

Figure 5 Comparative analysis of the DEJ zone of wild-type, *Fras1*$^{-/-}$ and *bl*/*bl* embryos. Confocal images of immunofluorescence staining with the indicated primary antibodies on sagittal cryosections of E15.5 (**a**–**d**,**g**–**j**) or E17.5 (**e**,**f**) embryos. Sections in **a**,**c**,**e**,**g** were prepared from wild-type embryos, in **b**,**d**,**f**,**h** from *Fras1*$^{-/-}$ embryos and in **i**,**j** from *bl*/*bl* embryos. All images represent comparable epidermal regions from the dorsal part of the embryos at the level of kidneys (from nonlesional regions of the mutants). Filled arrowheads demarcate the outer surface of the epithelial sheet of the epidermis and open arrowheads outline the fluorescence signal in the BMZ. (**a**) Fras1 is detected at the basal surface of epithelium in the DEJ zone in wild-type embryos. (**b**) Absence of Fras1 immunoreactivity in *Fras1*$^{-/-}$ mutants. (**c**,**d**) Laminin-α5 labels the skin BMZ of wild-type (**c**) and *Fras1*$^{-/-}$ mutants (**d**). (**e**,**f**) Detection of collagen VII in the BMZ (open arrowheads) of wild-type (**e**) and *Fras1*$^{-/-}$ mutants (**f**). (**g**) Collagen VI stains connective tissue cells and is confined to the dermal side of the skin BMZ in wild-type embryos. (**h**) Loss of collagen VI localization in the skin BMZ of *Fras1*$^{-/-}$ mutants. Staining is constricted solely to the connective tissue of the dermis. (**i**) The DEJ zone of *bl*/*bl* embryos is labeled by laminin-α5-specific antibodies and is devoid of Fras1 protein (**j**). Scale bar, 10 μm.

laminin α5, agrin and nidogen 1 followed the detached epithelium (**Fig. 6c–e**) and localized on the blister roof. Ultrastructural inspection of the detached epithelium by transmission electron microscopy mapped a well defined lamina lucida and lamina densa to the blister roof (**Fig. 6g**). Further ultrastructural details, like anchoring fibrils, were barely detectable below the lamina densa, as compared with wild-type (**Fig. 6f**), probably owing to the loss of attachment to the dermis and the extensive blood flow in the blister. Taken together, these data indicate that the cleavage plane is localized beneath the lamina densa. Hence, the absence of Fras1 probably affects the dermal-epidermal connection underneath the lamina densa, causing detachment and subepidermal blister formation. The split below the lamina densa possibly causes deeper intradermal ruptures that lead to vascular damage, explaining the hemorrhagic blisters.

The phenotypic characteristics of *Fras1*$^{-/-}$ mice phenocopy those of the existing blebbed mouse mutants[3,4]. Moreover, *bl*, one of the five blebbed mouse mutations, maps to chromosome 5, close to the *Fgf5* locus where *Fras1* also maps. This strongly argues that *Fras1* might be the gene that is affected by the *bl* mutation. Indeed, sequencing of coding exons from *bl*/*bl* genomic DNA identified a premature stop codon at amino acid 2,200 of Fras1 (ref. 6). Moreover, Fras1-specific antibodies verified the absence of Fras1 on

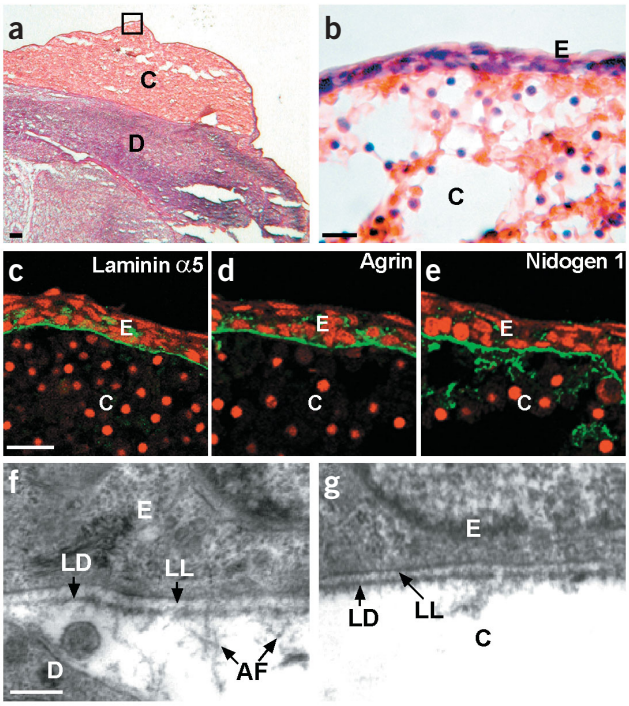

Figure 6 Analysis of the DEJ zone of blistered skin in *Fras1*$^{-/-}$ embryos. (**a**–**g**) Transverse cryosections through a blister over the eye region of an E15.5 *Fras1*$^{-/-}$ embryo. (**c**–**e**) Immunofluorescence staining of sections incubated with the indicated primary antibodies. (**a**,**b**) Hematoxylin and eosin post-staining of the above sections (**b** is a higher magnification of the squared area in **a**. (**c**–**e**) Confocal images from regions comparable to this area. Laminin α5, agrin and nidogen 1 are detected at the roof of the blister tip underneath the detached epithelium (**c**–**e**). (**f**,**g**) Transmision electron microscopy examination of the BMZ of a wild-type embryo (**f**) and of the blister roof (**g**) of an E15.5 *Fras1*$^{-/-}$ embryo bearing a hemorrhagic blister over the eye. Arrows point to the lamina lucida (LL), lamina densa (LD) and anchoring fibrils (AF) beneath the epithelium. C, blister cavity; D, dermis; E, epidermis. Scale bar in **a**,**b**, 100 μm; in **c**–**e**, 20 μm; and in **f**,**g**, 300 nm.

histological sections from *bl*/*bl* embryos, although other BMZ markers were normally detected (**Fig. 5i,j**). These data strongly suggest that mutations in *Fras1* are responsible for the *bl* phenotype. Furthermore, given the similarity between the phenotypes associated with *bl* and with *Fras1* inactivation, the *Fras1* mutation in *bl* mutants probably produces a null allele. The blebbed mutants have been proposed as an animal model for human Fraser syndrome[5,19]. Several parallels can be drawn between the primary phenotypic features of individuals with Fraser syndrome and the defects observed in *Fras1*$^{-/-}$ mutant mice. These include blister formation, syndactyly and eyelid fusion, and renal agenesis or dysplasia. This correlation is confirmed by the identification of several mutations in *FRAS1* in the individuals with Fraser syndrome[6].

METHODS

Isolation of *Fras1* cDNA. While searching for proteins that interact with Pax3, we selected one artificial cDNA clone (*Fras1*) based on the RNA expression pattern. Using this cDNA probe, we screened a mouse embryonic brain cDNA library constructed in the λExCell *Eco*RI/CIP vector and used overlapping fragments to assemble a nearly full-length *Fras1* cDNA (15,865 bp). A well defined Kozak sequence preceded by several in-frame stop codons, a polyadenylation signal and poly(A)$^+$ tail are present in the isolated sequence.

Northern-blot and RNA *in situ* analyses. We used a ^{32}P-labeled cDNA probe (*Eco*RI–*Bam*HI fragment, 896 bp) from the region encoding the VWC motifs of Fras1 to hybridize a northern blot containing poly(A)$^+$ RNA from different developmental stages of mouse embryos (Clontech Mouse Embryo MTN Blot). We used the same cDNA fragment to generate a RNA probe labeled with digoxigenin to hybridize 10-μm-thick cryosections of mouse embryos. We detected the signals with antibody against digoxigenin conjugated to alkaline phosphatase and NBT/BCIP substrates (Roche), according to manufacturer's guidelines.

Southern-blot analysis. We isolated mouse genomic DNA from tail biopsy samples, digested it with appropriate restriction enzymes and separated it by electrophoresis on agarose gels (7.5 μg per lane). We blotted DNA on Nylon Transfer Membranes (Schleicher & Schuell) and hybridized the blots with ^{32}P-labeled DNA probes (Random Priming).

Antibody preparation and purification. To generate a polyclonal antibody against Fras1, we immunized rabbits with a bacterially overexpressed peptide corresponding to amino acids 1,212–1,525 of Fras1. To purify the antibody, we incubated the immune serum with a nitrocellulose slice containing the blotted bacterial peptide and eluted specifically bound antibodies with 0.2 M glycine, pH 2.5.

Immunohistochemistry and TUNEL assays. After fixing embryos overnight in 4% paraformaldehyde in phosphate-buffered saline (PBS) and cryoprotection in 30% sucrose in PBS, we froze embryos in isopentane and stored them at –80 °C. For immunohistochemistry, we prepared 10-μm-thick cryosections, post-fixed them in acetone for 5 min, quenched endogenous peroxidase by incubation in 0.3% hydrogen peroxide in 50% methanol/50% PBS for 15 min and incubated with primary antibody overnight at 4 °C and with biotinylated secondary antibody (VECTASTAIN Elite ABC Kit) for 2 h at room temperature. We used a peroxidase substrate solution DAB (diaminobenzidine, Sigma) to visualize staining. Alternatively, after overnight incubation with the primary antibody, we used a fluorescence-labeled secondary antibody (Alexa 594, Molecular Probes) and counterstained cell nuclei with propidium iodide. We carried out TUNEL assays using the In-Situ Cell Death Detection Kit-Flourescein (Roche) on cryosections of E14.5 mouse embryos according to the manufacturer's guidelines.

Histology. After dissection, we fixed embryos in 4% paraformaldehyde in PBS at 4 °C, dehydrated them, cleared them with xylene and embedded them in paraffin. We stained 10-μm sections with cresyl violet or hematoxylin and eosin using standard procedures.

Electron microscopy. For transmission electron microscopy, we fixed E15.5 mouse embryos in 2% glutaraldehyde/2% paraformaldehyde, post-fixed them in 2% aqueous osmium tetraoxide, stained them with 2% tannic acid for 60 min, dehydrated them and embedded them in a modified Mollenhauer's resin[20]. We used uranyl acetate and lead citrate to post-stain ultrathin sections and obtained images on a JEOL 100C Electron Microscope operating at 100 kV.

Generation of *Fras1*$^{-/-}$ mice. We screened a mouse 129/OLA genomic library constructed in the λGEMTM-12 vector (provided by A. Berns, The Netherlands Cancer Institute, NKI) using a 700-bp DNA fragment from the 5′ end of the translated region of the *Fras1* cDNA. In the targeting construct, 2.6-kb-upstream and 10.3-kb-downstream *Fras1* genomic sequences flanked an expression cassette containing *lacZ* (encoding β-galactosidase) fused in-frame to *Fras1* coding sequence and the RSV promoter that controls the expression of *neo* (encoding neomycin; pGNA-vector[21]). We transfected R1 mouse embryonic stem (ES) cells with the targeting construct and analyzed genomic DNA from G418-resistant clones (203) for homologous recombination by Southern blotting using an external probe. We used internal probes in Southern blots to verify the single integration of the targeting construct (data not shown). We obtained four independently targeted ES cell lines and generated chimeric males by aggregation of ES cells to NMRI morulae. One of the ES clones transmitted efficiently the targeted allele to the germ line. We maintained the introduced mutation on both an inbred (C57BL/10) and an outbred (NMRI) mouse strain and carried out the entire phenotypic analysis in the F_5 generation. Newborn homozygous mice on the NMRI background are comparable in body size to their wild-type and heterozygous littermates and start showing growth retardation after birth. After three months, they start recovering and are viable and fertile. We could not use the *lacZ* integrated into the *Fras1* locus as a marker for endogenous *Fras1* expression, although we observed staining with antibodies specific to β-galactosidase (data not shown).

Radiation hybrid mapping and data analysis. For chromosomal localization of *FRAS1*, we screened by PCR the radiation hybrid panels G3 and GB4, and for localization of *Fras1* the radiation hybrid panel T31 (panels were purchased from Research Genetics). We analyzed radiation hybrid data (retention patterns) from the T31, G3 and GB4 panels with the RHMAP3.0 software package. We analyzed G3 and GB4 radiation hybrid data by submitting the retention pattern to the G3 server at Stanford and to the GB4 server at MIT, respectively. Primer sequences for PCR are available on request.

Accession number. *Fras1*, AJ489280.

ACKNOWLEDGMENTS

We thank S. Meyer and S. Mahsur for help with the mouse stem cells and morula aggregation; E. Pavlakis for technical assistance; R. Timpl for the antibodies for laminin α5, laminin γ1, agrin and nidogen 1; P. Bonaldo for the collagen VI antibody; L. Bruckner-Tuderman for collagen VII antibodies; H. Krambovitis for the generation of Fras1 antibodies; L. Panagis, C. Dermon and G. Mavrothalassitits for help with the TUNEL assay; A. Argyrokastritis and S. Theophilou for critical reading of the manuscript; and P. Gruss for providing expertise and facilities of his laboratory. This work was supported by a grant from the Greek General Secretariat for Science and Technology and the British Heart Foundation (to P.J.S.).

COMPETING INTERESTS STATEMENT

The authors declare that they have no competing financial interests.

Received 22 April; accepted 5 May 2003
Published online 25 May 2003; doi:10.1038/ng1168

1. Bruckner-Tuderman, L. & Bruckner, P. Genetic diseases of the extracellular matrix: more than just connective tissue disorders. *J. Mol. Med.* **76**, 226–237 (1998).
2. Gustafsson, E. & Fassler, R. Insights into extracellular matrix functions from mutant mouse models. *Exp. Cell Res.* **261**, 52–68 (2000).
3. Darling, S. & Gossler, A. A mouse model for Fraser syndrome? *Clin. Dysmorph.* **3**, 91–95 (1994).
4. Lyon, M.F., Rastan, S. & Brown, S.D. *Genetic Variants and Strains of the Laboratory Mouse* 3rd edn. (Oxford University Press, New York, 1996).
5. Winter, R.M. Fraser syndrome and mouse "*bleb*" mutants. *Clin. Genet.* **37**, 494–495 (1990).
6. McGregor, L. *et al.* Fraser syndrome and mouse blebbed phenotype caused by mutations in *FRAS1*/*Fras1* encoding a putative extracellular matrix protein. *Nat. Genet.*

34, '–' (2003). **[Ed: page numbers for Scambler]**
7. Sadler, J.E. Biochemistry and genetics of von Willebrand factor. *Annu. Rev. Biochem.* **67**, 395–424 (1998).
8. Roebroek, A.J.M. *et al*. Cloning and functional expression of Dfurin2, a Subtilisin-like proprotein processing enzyme of *Drosophila melanogaster* with multiple repeats of a cysteine motif. *J. Biol. Chem.* **267**, 17208–17215 (1992).
9. Nishiyama, A., Dahlin, K.J., Price, J.T., Johnstone, S.R. & Stallcup, W.B. The primary structure of NG2, a novel membrane-spanning proteoglycan. *J. Cell Biol.* **114**, 359–371 (1991).
10. Schwarz, E.M. & Benzer, S. *Calx*, a Na-Ca exchanger gene in *Drosophila melanogaster*. *Proc. Natl. Acad. Sci. USA* **94**, 10249–10254 (1997).
11. Hodor, P.G., Illies, M.R., Broadley, S. & Ettensohn, C.A. Cell-substrate interactions during sea urchin gastrulation: migrating primary mesenchyme cells interact with and align extracellular matrix fibers that contain ECM3, a molecule with NG2-like and multiple calcium-binding domains. *Dev. Biol.* **222**, 181–194 (2000).
12. Spirito, F. *et al*. Reduced expression of the epithelial adhesion ligand laminin 5 in the skin causes intradermal tissue separation. *J. Biol. Chem.* **276**, 18828–18835 (2001).
13. Arin, M.J. & Roop, D.R. Disease model: heritable skin blistering. *Trends Mol. Med.* **7**, 422–424 (2001).
14. McGowan, K.A. & Marinkovich, M.P. Laminins and human disease. *Microsc. Res. Tech.* **51**, 262–279 (2000).
15. Kuure, S., Vuolteenaho, R. & Vainio, S. Kidney morphogenesis: cellular and molecular regulation. *Mech. Dev.* **92**, 31–45 (2000).
16. Muller, U. *et al*. Integrin α8β1 is critically important for epithelial-mesenchymal interactions during kidney morphogenesis. *Cell* **88**, 603–613 (1997).
17. Willem, M. *et al*. Specific ablation of the nidogen-binding site in the laminin gamma1 chain interferes with kidney and lung development. *Development* **129**, 2711–2722 (2002).
18. Tillet, E., Ruggiero, F., Nishiyama, A. & Stallcup, W.B. The membrane-spanning proteoglycan NG2 binds to collagens V and VI through the central nonglobular domain of its core protein. *J. Biol. Chem.* **272**, 10769–10776 (1997).
19. Slavotinek, A.M. & Tifft, C.J. Fraser syndrome and cryptophthalmos: review of the diagnostic criteria and evidence for phenotypic modules in complex malformation syndromes. *J. Med. Genet.* **39**, 623–633 (2002).
20. Snyder, P.B., Galanopoulos, V.K. & Kafatos, F.C. *Trans*-acting amplification mutants and other eggshell mutants of the third chromosome in *Drosophila melanogaster*. *Proc. Natl. Acad. Sci. USA* **83**, 3341–3345 (1986).
21. Mouellic, H.L., Lallemand, Y. & Brulet, P. Targeted replacement of the Homeobox gene *Hox-3.1* by the *Escherichia coli LacZ* in mouse chimeric embryos. *Proc. Natl. Acad. Sci. USA* **87**, 4712–4716 (1990).